Manuscript prepared for Geosci. Model Dev. Discuss.
with version 2014/09/16 7.15 Copernicus papers of the LaTeX class copernicus.cls.
Date: 19 February 2016

DebrisInterMixing-2.3: a Finite Volume solver for three dimensional debris flow simulations based on a single calibration parameter – Part 1: Model description

A. von Boetticher[1,3], **J. M. Turowski**[2,3], **B. W. McArdell**[3], **D. Rickenmann**[3], **and J. W. Kirchner**[1,3]

[1]Department of Environmental Systems Science, ETH Zentrum, CHN H41, 8092 Zürich, Switzerland
[2]Helmholtz-Centre Potsdam GFZ German Research Center for Geosciences, Telegrafenberg, 14473 Potsdam, Germany
[3]Swiss Federal Research Institute WSL, Zürcherstrasse 111, 8903 Birmensdorf, Switzerland

Correspondence to: A. von Boetticher (albrecht.vonboetticher@usys.ethz.ch)

Abstract

Here we present a three-dimensional fluid dynamic solver that simulates debris flows as a mixture of two fluids (a Coulomb-Viscoplastic model of the gravel mixed with a Herschel-Bulkley representation of the fine material suspension) in combination with an additional unmixed phase representing the air and the free surface. We link all rheological parameters to the material composition, i. e., to water content, clay content and mineral composition, content of sand and gravel, and the gravel's friction angle; the user must specify only a single free model parameter. The Volume-of-Fluid (VOF) approach is used to combine the mixed phase and the air phase into a single cell-averaged Navier-Stokes equation for incompressible flow, based on code adapted from standard solvers of the Open-Source CFD software OpenFOAM. The VOF method saves computational costs compared to drag-force based multiphase models. Thus depth-averaging is not necessary and complex three-dimensional flow structures can be simulated while accounting for the pressure- and shear-rate-dependent rheology.

1 Introduction

Debris flows typically occur in steep mountain channels. They are characterized by unsteady flows of water together with different contents of clay, silt, sand, gravel, and larger particles, resulting in a dense and often rapidly moving fluid mass. They are often triggered by heavy rainfall and can cause massive damage (Petley et al., 2007; Hilker et al., 2009). Their importance has increased due to intense settlement in mountainous regions and also due to their sensitivity to climate change (Guthrie et al., 2010). Their damage potential is not limited to direct impact; severe damage can also be caused by debris flows blocking channels and thus inducing over-topping of the banks by subsequent flows.

Modeling debris flows is a central part of debris-flow research, because measuring the detailed processes in debris-flow experiments or in the field is challenging. It is still uncertain how laboratory tests can be scaled to represent real flow events, and the inhomogeneous

mixture of gravel and fine material brings about interactions of granular flow and viscous forces like drag and pore-pressure that are difficult to track with the present measurement techniques at reasonable cost. As a consequence, the rheological behavior of debris flow material is incompletely understood.

Typically, current numerical modeling approaches cannot predict run-out distances or impact pressures of debris flows in known terrain without prior parameter calibration, based on simulating previous well-documented events that happened at the same site. This clearly represents a challenge in practical applications, because reliable calibration data are rarely available. In addition, the interactions between the granular and fluid phases, and the dynamic change in granular and fluid concentrations during the flow process, limit simple models to the narrow range of simulations that they have been calibrated for, where the fitted parameters account for these interactions. Complex models such as depth-averaged fluid simulations coupled to three dimensional particle methods are associated not only with high computational costs but also with a large number of model parameters, making model calibration the key issue for application to specific cases. This limits the possibilities of using debris flow models as a valid standard application in practice, because the user's ability to estimate values of poorly constrained parameters influences the results.

Here, we present an improved multiphase modeling approach as an alternative. We provide a coarse but effective solution linking the rheological model of the debris-flow material to field values such as grain size distribution and water content. The approach aims to link the knowledge of field experts for estimating the release volume and material composition with recent advances that account for complex flow phenomena using three-dimensional computational fluid dynamics. The parameters of the two resulting rheology models for the two mixing fluids are linked to material properties such that the model setup can be based on material samples collected from the field, yielding a model that has only one free parameter for calibration. One mixing phase represents the suspension of finer particles with water (also simply called slurry in this paper) and a second mixing phase accounts for the pressure-dependent flow behavior of gravel. A third gas phase is kept unmixed to model the free surface. The focus is on the flow and deposition process and the release body needs

to be user-defined. Although, some aspects of material mobilization can be addressed by locally altering the concentration of the slurry phase and the water content of the slurry defined in the material properties, this is not within the scope of this paper.

Table 1. Nomenclature

α	phase fraction
α_m	fraction of the debris mixture (slurry + gravel)
$\boldsymbol{U}$	velocity
$\boldsymbol{Uc}$	inter-facial compression velocity
t	= time
$\mathbf{T}$, $\mathbf{T_s}$	deviatoric viscous stress tensor (s for granular phase)
$\mathbf{D}$	strain rate tensor
ρ	phase-averaged density, $\rho_i (i = 1,2,3)$ density of phase i, ρ_{exp} is a bulk density in experiment
p, p_d	pressure resp. modified pressure
D_{diff}	diffusion constant
ϕ	volumetric flux (ϕ_ρ denotes mass flux, ϕ_r a surface-normal flux)
$\mathbf{I}$	identity matrix
μ	phase-averaged dynamic viscosity, $\mu_i (i = 1,2,3)$ viscosity of phase i
μ_0	maximal dynamic viscosity
μ_{min}	minimal dynamic viscosity
μ_s	Coulomb-viscoplastic dynamic viscosity
∇	gradient
σ	free surface tension coefficient
κ	free surface curvature
$\boldsymbol{g}$	gravitational acceleration
τ	shear stress
τ_y	yield stress of slurry phase (τ_{y-exp} is a measured yield stress)
k	Herschel-Bulkley consistency factor
n	Herschel-Bulkley exponent
$\dot{\gamma}$	shear rate
C	volumetric solid concentration
P_0	volumetric clay concentration
P_1	reduced P_0 in case of high clay content
τ_{00}	free model parameter (affects slurry phase rheology)
τ_0	modified τ_{00} in case of high C
τ_{0s}	yield stress of granular phase modeled with Coulomb friction
β	slope angle
δ	internal friction angle approximated as angle of repose
m_y	constant model parameter (would affect gravel phase rheology)

2 Modeling approach

The debris flow material can be subdivided into a combination of a granular phase mixed with an interstitial fluid composed of the fine material suspension. The latter was successfully modeled in the past as a shear-rate dependent Herschel-Bulkley fluid (Coussot et al., 1998). Because pressure and shear drive the energy dissipation of particle-to-particle contacts, the shear rate substantially influences the energy dissipation within the granular phase. While the two-phase models of Iverson and Denlinger (2001) and Pitman and Le (2005) treated the granular phase as a shear-rate independent Mohr-Coulomb plastic material, dry granular material has been successfully modeled as a viscoplastic fluid by Ancey (2007), Forterre and Pouliquen (2008), Balmforth and Frigaard (2007) and Jop et al. (2006). We follow the suggestions given by Pudasaini (2012) to account for the non-Newtonian behavior of the fluid and the shear- and pressure-dependent Coulomb-viscoplastic behavior of the granular phase, as applied by Domnik et al. (2013). Several modeling approaches to account for the two-phase nature of debris flows used depth-averaged Navier-Stokes equations for each phase coupled by drag models (eg. Bozhinskiy and Nazarov (2000), Pitman and Le (2005), Pudasaini (2012) and Bouchut et al. (2015)). We apply the numerically more efficient method of Iverson and Denlinger (2001) and treat the debris flow material as one mixture with phase-averaged properties described by a single set of Navier-Stokes equations. The resulting reduction in numerical costs allows us to model the three-dimensional momentum transfer in the fluid as well as the free-surface flow over complex terrain and obstacles.

Multiphase flows of gas, fluid and sediment can be addressed with the so-called mixture- or drift-flux model in cases where the local difference in phase velocities is small (Bohorquez, 2008). The properties of all phases are cell-averaged to derive a single mass continuity and momentum balance equation describing the entire mixture. The model presented here has to be seen as a first step, assuming that the local velocity of the gravel is about the same as the velocity of the surrounding fluid, thus allowing us to neglect the drift-flux. This assumption would not be valid for debris flows with little interstitial fluid, or with

interstitial fluid of small viscosity (i. e., a slurry with low concentrations of fine material). The assumption of equal velocities of both phases in one cell leads to a constant composition of the mixture by means of phase concentrations over the entire flow process. This basic model can be seen as a counterpart to the mixture model of Iverson and Denlinger (2001), extended by resolving the three dimensional flow structure in combination with a pressure- and shear-rate-dependent rheology linked to the material composition. In future work, we aim to relax the constraint of equal phase velocities and allow dispersion of constituents by introducing relative velocities of the gravel phase with respect to the fine sediment suspension according to Bohorquez (2012) and Damián (2013) together with a coupled Lagrangian particle simulation that can account for larger grains. The basic model presented here focuses on the role of pressure-dependent flow behavior of the gravel, in combination with the shear-dependent rheology of the slurry.

We base our model concept on the well-established finite volume solver interFoam, which is designed for incompressible two-phase flow simulations of immiscible fluids (Deshpande et al., 2012). A standard extension named interMixingFoam introduces two mixing phases without momentum exchange coupled to a third unmixed phase by surface tension. Numerical costs are kept reasonable due to the Volume-of-Fluid (VOF) method (Hirt and Nichols, 1981), which solves only one Navier-Stokes equation system for all phases. The viscosity and density of each grid cell is calculated as a concentration-weighted average between the viscosities of the phases that are present in the cell. Between the two mixing phases of gravel and slurry, the interaction reduces to this averaging of density and viscosity. In this way, the coupling between driving forces, topography and three dimensional flow-dependent internal friction can be addressed for each phase separately, accounting for the fundamental differences in flow mechanisms of granular and viscoplastic fluid flow that arise from the presence or absence of Coulomb friction (Fig. 1). We apply linear concentration-weighted averaging of viscosities for estimating the bulk viscosity of a mixture for simplicity. Non-linear averaging of viscosity between phases as suggested by Gao and Li (2012) may be introduced in the future.

2.1 Governing Equations

Assuming isothermal incompressible phases without mass transfer, we separate the modeled space into a gas region denoting the air and a region of two mixed liquid phases. The VOF method used here determines the volume fractions of all phases in an arbitrary control volume by using an indicator function which yields a phase fraction field for each phase. The phase fraction field represents the probability that a phase is present at a certain point in space and time (Hill, 1998). The air fraction may be defined in relation to the fraction of the mixed fluid α_m as

$$\alpha_1 = 1 - \alpha_m \tag{1}$$

and the mixed fluid α_m may be defined as the sum of the constant fractions of the mixing phases α_2 and α_3:

$$\alpha_m = \alpha_2 + \alpha_3. \tag{2}$$

The flow is defined by the continuity equation together with the transport and momentum equations:

$$\nabla \cdot \boldsymbol{U} = 0, \tag{3}$$

$$\frac{\partial \alpha_m}{\partial t} + \nabla \cdot (\boldsymbol{U} \alpha_m) = 0, \tag{4}$$

and

$$\frac{\partial (\rho \boldsymbol{U})}{\partial t} + \nabla \cdot (\rho \boldsymbol{U} \times \boldsymbol{U}) = -\nabla p + \nabla \cdot \mathbf{T} + \rho \boldsymbol{f}, \tag{5}$$

where $\boldsymbol{U}$ represents the velocity field shared by all phases, $\mathbf{T}$ is the deviatoric viscous stress tensor, ρ is the phase-averaged density, p denotes pressure and $\boldsymbol{f}$ stands for body forces per unit mass like gravity.

An efficient technique of the VOF method is to convect the phase fraction field α_m as an invariant with the divergence-free flow field $\boldsymbol{U}$ that is known from previous time steps:

$$\frac{\partial \alpha_m}{\partial t} + \nabla \cdot (\boldsymbol{U}\alpha_m) + \nabla \cdot (\alpha_1 \boldsymbol{U_c}) = 0, \tag{6}$$

where t denotes time and $\boldsymbol{U_c}$ is an artificial inter-facial compression velocity acting perpendicular to the interface between the gas region and the mixed liquid phases. The method allows a reconstruction of the free surface with high accuracy if the grid resolution is sufficient (Berberović et al., 2009; Hoang et al., 2012; Deshpande et al., 2012; Hänsch et al., 2013). The details about the interface compression technique, the related discretization and numerical schemes to solve eq. 6 are given in Deshpande et al. (2012). However, to allow evolving phase concentrations between the mixing phases of the slurry α_2 and the gravel α_3 in future releases, our modified version of the interMixingFoam solver applies eq. 6 separately to each mixing phase including diffusion:

$$\frac{\partial \alpha_i}{\partial t} + \nabla \cdot (\boldsymbol{U}\alpha_i) - D_{diff}\nabla^2 \alpha_i + \nabla \cdot (\alpha_1 \boldsymbol{U_c}) = 0, \tag{7}$$

where $i = 2, 3$ denote the slurry and gravel phases and D_{diff} is the diffusion constant that is set to a negligible small value within the scope of this paper.

The discrete form of eq. 7 is derived by integrating over the volume V of a finite cell of a grid-discretization of the simulated space, which is done in the finite volume method by applying the Gauss Theorem over the cell faces. The advective phase fluxes $\phi_{1..3}$ are obtained by interpolating the cell values of α_1, α_2 and α_3 to the cell surfaces and by multiplying them with the flux ϕ through the surface, which is known from the current velocity field. To keep the air phase unmixed, it is necessary to determine the flux ϕ_r through the interface between air and the debris flow mixture, and to subtract it from the calculated phase fluxes

$\phi_{1..3}$. Inherited from the original interMixingFoam solver (OpenFOAM-Foundation, 2016a), limiters are applied during this step to bound the fluxes to keep phase concentrations between 0 and 1. With known fluxes $\phi_{1..3}$, the scalar transport equation without diffusion for each phase takes the form

$$\frac{\partial}{\partial t}\alpha_i + \nabla(\phi_i) = 0. \tag{8}$$

Equation 8 is solved using first-order Euler schemes for the time derivative terms, as has been recommended for liquid column breakout simulations (Hänsch et al., 2013).

After solving the scalar transport equations, the complete mass flux ϕ_ρ from the updated volumetric phase concentrations is constructed:

$$\phi_\rho = \phi_1 \cdot \rho_1 + \phi_2 \cdot \rho_2 + \phi_3 \cdot \rho_3, \tag{9}$$

where $\rho_{1..3}$ denote the constant densities of the corresponding phases and $\phi_{1..3}$ are the corresponding fluxes.

Fig. 2 illustrates how the phase volume distributions α_1 (air), α_2 (slurry) and α_3 (gravel) are used to derive cell-averaged properties of the continuum.

The conservation of mass and momentum is averaged with respect to the phase fraction α of each phase. The density field is defined as

$$\rho = \sum_i \rho_i \alpha_i \tag{10}$$

where ρ_i denotes density of phase i and the density is assumed to be constant.

The deviatoric viscous stress tensor **T** is defined based on the mean strain rate tensor **D** that denotes the symmetric part of the velocity gradient tensor derived from the phase-averaged flow field:

$$\mathbf{D} = \frac{1}{2}[\nabla \boldsymbol{U} + (\nabla \boldsymbol{U})^T], \tag{11}$$

and

$$\mathbf{T} = 2\mu\mathbf{D} - \frac{2}{3}\mu(\nabla \cdot \boldsymbol{U})\mathbf{I}. \tag{12}$$

I is the identity matrix and μ is the phase-averaged dynamic viscosity, which is simplified in analogy to eq. 10 as the concentration-weighted average of the corresponding phase viscosities:

$$\mu = \sum_i \mu_i \alpha_i \tag{13}$$

The term $\nabla \cdot \mathbf{T}$ in the momentum equation 5 is decomposed as $\nabla \cdot (\mu \nabla \boldsymbol{U}) + \nabla \boldsymbol{U} \cdot \nabla \mu$ to ease discretization. The body forces $\boldsymbol{f}$ in the momentum equation account for gravity and for the effects of surface tension. The surface tension at the interface between the debris flow mixture and air is modeled as a force per unit volume by applying a surface tension coefficient σ. The momentum conservation including gravitational acceleration $\boldsymbol{g}$ and surface tension is defined in our model as:

$$\frac{\partial(\rho \boldsymbol{U})}{\partial t} + \nabla \cdot (\rho \boldsymbol{U} \times \boldsymbol{U}) = -\nabla p_d + \nabla \cdot (\mu \nabla \boldsymbol{U}) + (\nabla \boldsymbol{U}) \cdot \nabla \mu - \boldsymbol{g} \cdot \boldsymbol{x} \nabla \rho + \sigma \kappa \nabla \alpha_1 \tag{14}$$

where κ denotes the local inter-facial curvature and $\boldsymbol{x}$ stands for position. The modified pressure p_d is employed in the solver to overcome some difficulties with boundary conditions in multiphase flow simulations. In case the free surface lies within an inclined wall

forming a no-slip boundary condition, the normal component of the pressure gradient must be different for the gas phase and the mixture due to the hydrostatic component ρg. It is common to introduce a modified pressure p_d related to the pressure p by

$$p_d = p - \rho \boldsymbol{g} \cdot \boldsymbol{x}. \tag{15}$$

The gradient of the modified pressure includes the static pressure gradient and contributions that arise from the density gradient as well as a body force due to gravity (Berberović et al., 2009).

Together with the continuity equation 3 for the multi-phase flow, eq. 14 allows us to calculate the pressure and gravity driven velocities. The corresponding discretization and solution procedure with the PISO (Pressure-Implicit with Splitting of Operators (Issa, 1986)) algorithm is provided in appendix A. In the following section we present the rheology models that define the viscosity components for eq. 13.

2.2 Rheology model for the fine sediment suspension

The viscosity of the gas phase, μ_1 is chosen constant. The introduction of two mixing phases is necessary to distinguish between the pressure-dependent flow behavior of gravel and the shear-thinning viscosity of the suspension of finer particles with water. The rheology of mixtures of water with clay and sand can be described by the Herschel-Bulkley rheology law (Coussot et al., 1998), which defines the shear stress in the fluid as:

$$\tau = \tau_y + k\dot{\gamma}^n \tag{16}$$

where τ_y is a yield stress below which the fluid acts like a solid, k is a consistency factor for the viscosity of the sheared material, $\dot{\gamma}$ is the shear rate and n defines the shear-thinning

($n < 1$) or shear-thickening ($n > 1$) behavior. In OpenFOAM, the shear rate is derived in 3D from the strain rate tensor **D**:

$$\dot{\gamma} = \sqrt{2 \cdot \mathbf{D} : \mathbf{D}} \tag{17}$$

The shear rate is based on the strain rate tensor to exclude the rotation velocity tensor that does not contribute to the deformation of the fluid body. The model can be rewritten as a generalized Newtonian fluid model to define the shear-rate-dependent effective kinematic viscosity of the slurry phase as:

$$\mu_2 = k|\dot{\gamma}|^{n-1} + \tau_y|\dot{\gamma}|^{-1} \tag{18}$$

if the viscosity is below an upper limit μ_0 and

$$\mu_2 = \mu_0 \tag{19}$$

if the viscosity is higher, to ensure numerical stability.

With $n = 1$ the model simplifies to the Bingham rheology model that has been widely used to describe debris-flow behavior in the past. It may be reasonable to imagine the rheology parameters to be dependent on the state of the flow. However, even with the implicit assumption that the coefficients are a property of the material and not of the state of the flow, the Herschel-Bulkley rheology law was rarely applied in debris-flow modeling due to the large number of rheology parameters. We avoid this problem by assuming the rheology parameters to be defined by measurable material properties as described below.

2.2.1 Determination of rheology model parameters based on material properties

Results from recent publications allow the reduction of the number of free Herschel-Bulkley parameters to one. If the coarser grain fraction is confined to the gravel phase, the Herschel-Bulkley parameters for the finer material can be linked to material properties as measured

using simple standard geotechnical tests. According to Coussot et al. (1998), the exponent n can be assumed constant as $1/3$, and k can be roughly estimated as $b \cdot \tau_y$, where the constant $b = 0.3\text{s}^{-\text{n}}$ for mixtures with maximum grain-sizes < 0.4 mm (Coussot et al., 1998). An approach for estimating the yield stress τ_y based on water content, clay fraction and composition, and the solid concentration of the entire debris flow material was proposed by Yu et al. (2013) as:

$$\tau_y = \tau_0 C^2 e^{22(C \cdot P_1)} \tag{20}$$

where C is the volumetric solid concentration of the mixture, $P_1 = 0.7P_0$ when $P_0 > 0.27$ and $P_1 = P_0$ if $P_0 <= 0.27$, and

$$P_0 = C_{kaolinite+chlorite} + 1.3C_{illite} + 1.7C_{montmorillonite} \tag{21}$$

where the subscript of C refers to the volumetric concentration (relative to the total volume of all solid particles and water) of the corresponding mineral. The discontinuity of P_1 at a modified clay concentration of $P_0 = 0.27$ is a coarse adjustment to a more-or-less sudden change observed in the experimental behavior.
For $C < 0.47$, τ_0 is equal to τ_{00} and otherwise τ_0 can be calculated by

$$\tau_0 = \tau_{00} e^{5(C-0.47)} \tag{22}$$

where τ_{00} is the remaining free parameter which we use to account for the grid size dependency of the shear rate (Yu et al., 2013). We recommend a value of $\tau_{00} = 30$ Pa as a starting point for calibration. Yu et al. (2013) compared this method of estimating the yield stress τ_y to experimental results they obtained from a set of 514 flume experiments with mixtures of water and clay with fine and coarse sand and less than 5 % gravel. They determined the yield stress by releasing the material mixture from a reservoir into an inclined channel of

0.2 m width and by increasing the inclination slightly until remobilization occurred after the material came to rest. The experimental yield stress τ_{y-exp} was then determined as:

$$\tau_{y-exp} = \rho_{exp} g h sin(\beta), \tag{23}$$

where ρ_{exp} is the density of the applied mixture, g the acceleration due to gravity, h the maximum accumulation thickness of the deposit, and β the slope inclination. In addition, they compared the calculated yield stress of eq. 20 with experimental yield stresses reported by a number of authors including Coussot et al. (1998) and Ancey and Jorrot (2001). Ancey and Jorrot (2001) used 2 mm and 3 mm glass beads in a kaolinite dispersion as well as fine sand-kaolinite-water mixtures. Up to yield stresses of about 200 Pa the yield stresses estimated by eq. 20 fit the observed ones well. Thus, the yield stresses of sand-clay mixtures with water can be estimated using eq. 20 based on the volumetric concentration of the debris in the water-solids mixture and based on the percentages of different clays in the fraction of fine material. Adjustments to the numbers for calculating P_0 may be necessary to account for the activity of other clays.

The remaining uncertainties concern our assumptions that n is constant at a value of $1/3$, and that k can be defined in such simple dependency to τ_y in the presence of coarser sand. Experiments seem to confirm that n increases in presence of coarser material (Imran et al., 2001), but further research is needed to quantify this effect. Remaitre et al. (2005) found n to vary from 0.27 to 0.36. Schatzmann et al. (2003) used $n = 0.33$ to reproduce measured curves obtained with a mixture of 27.5 volumetric percent slurry with 30 % gravel where gravel grain-sizes ranged from 3 to 10 mm, and used $n = 0.5$ to fit the Herschel-Bulkley model to the experiment with 22.5 % slurry and 30 % gravel. Based on the laboratory scale experiments that are presented in v. Boetticher et al. (2015) we have chosen $n = 0.34$ to obtain the best fit for the simulation presented by large-scale debris-flow experiments.

2.3 Representation of gravel by a Coulomb-viscoplastic rheology

During acceleration and high-speed flow, the shear-thinning behavior of both the fluid and the granular phase dominate the viscosity in our model. However, pressure-dependent friction becomes important as soon as the material experiences high pressures, accompanied by reduction in shear due to decelerations caused by channel slope reduction. Flows of granular material could be modeled as viscoplastic fluids (Ancey, 2007; Forterre and Pouliquen, 2008; Balmforth and Frigaard, 2007; Jop et al., 2006) as cited by Domnik and Pudasaini (2012). Based on Ishii (1975), the granular stress deviator tensor $\mathbf{T_s}$ can be written as:

$$\mathbf{T_s} = -\frac{p}{\rho}\mathbf{I} + 2\mu_s\mathbf{D}, \tag{24}$$

where $p\mathbf{I}$ is the pressure times the identity matrix and μ_s is the corresponding dynamic viscosity, which was modeled by Domnik and Pudasaini (2012) as:

$$\mu_s = \mu_{min} + \frac{\tau_{0s}}{||\mathbf{D}||}[1 - e^{-m_y||\mathbf{D}||}], \tag{25}$$

where μ_{min} is a minimal dynamic viscosity, τ_{0s} is a yield stress, and $||\mathbf{D}||$ is the norm of the strain-rate tensor defined by the authors as:

$$||\mathbf{D}|| = \sqrt{2tr(\mathbf{D}^2)}. \tag{26}$$

In eq. 25, m_y is a model parameter with units of s which we will keep constant, for reasons outlined in the following section. Domnik et al. (2013) suggested replacing the yield stress by a pressure-dependent Coulomb friction, $psin(\delta)$ where δ is the internal friction angle:

$$\mu_3 = \mu_{min} + \frac{psin(\delta)}{\rho_3||\mathbf{D}||}[1 - e^{-m_y||\mathbf{D}||}] \tag{27}$$

Here, this Coulomb-viscoplastic rheology model is used to describe the gravel phase. The pressure- and shear-dependent viscosity is calculated in every cell with the corresponding local pressure p and strain-rate tensor **D** derived from the phase-averaged flow field.

2.3.1 Gravel phase properties

The Coulomb-viscoplastic rheology law developed by Domnik et al. (2013) includes two parameters: the friction angle δ, and the parameter m_y influencing the transition between yielded and unyielded regions. For smaller values of m_y, the transition is smoother. In the absence of shear, to achieve a viscosity representing a Coulomb friction equal to $p \cdot sin(\delta)$ where p is the local pressure, m_y needs to be equal to 1 s. However, the development of μ_s under large pressure or strong shear is the same for both $m_y = 1$ s and $m_y = 0.2$ s, but parts of the nearly immobile material that face little pressure (in general, immobile material close to the surface) show a significant reduction in viscosity when $m_y = 0.2$ s (Fig. 3). As a consequence, m_y minimally affects debris flow release and flow at large scales, but material with a shallow flow depth in a run-out plane close to deposition may develop front fingering (which is dependent on, and sensitive to, the value of m_y) by allowing sudden local solidification. We choose m_y to be constant and equal to 0.2 s for all simulations.
For small friction angles, the modeled viscosity of the gravel phase decreases rapidly with increasing shear. Larger friction angles increase the viscosity and extend the pressure dependency to larger shear rates (Fig. 4). We estimated the friction angle δ based on the maximum angle of repose in tilt-table tests of the gravel. In our laboratory experiments, we determined the friction angle in a simple adaptation of the method of Deganutti et al. (2011) by tilting a large box with loose material until a second failure of the material body occurred.

In analogy to the Herschel-Bulkley implementation, an upper limit for the viscosity is implemented to maintain numerical stability. Pressure-dependent viscosity in the incompressible Navier-Stokes equations causes numerical instability as soon as the eigenvalues of the symmetric part of the local velocity gradient become larger than $1/(2(\delta\mu/\delta p))$. Following Renardy (1986), we locally limit the viscosity to keep it below a corresponding local stability limit.

3 Quality characteristics of the model

3.1 Effects of time step size on rheology

Because most debris-flow models are depth-averaged and use shallow-water approximations, one could ask why a three-dimensional approach is necessary. Brodani-Minussi and deFreitas Maciel (2012) compared dam-break experiments of a Herschel-Bulkley fluid and its numerical simulations using the VOF approach with published shallow-water-equation-based models. Especially for the first instant after the material release, the application of shallow-water equations seems to introduce errors that are propagated throughout the process, leading to erroneous run-out estimates. A similar problem arises when modeling debris-flow impacts on obstacles. Simulating the impact of material with velocity-dependent rheology that is kept constant over the time step although it actually changes with the changing flow leads to an accumulating over- or underestimation of energy dissipation. In our model, during release of immobile material that accelerates, the viscosity is overestimated over each time step. As a consequence, the velocity at the end of the time step is underestimated, which again amplifies the overestimation of viscosity in the next time step. Conversely, at an impact, the sudden deceleration causes an underestimation of viscosity over the time step length, leading to an overestimated velocity that again amplifies the underestimation of the viscosity in the next time step. As a result, flow velocities change with changing time step size. Avalanche codes such as RAMMS (Christen et al., 2007) deal with this problem by calibrating the model to data from previous events at the same location and similar conditions. But changes in release volume or position can lead to different accelerations and corresponding changes in the automatic time step control can alter the development of rheology over time. As long as a flow stage is reached where the flow stops accelerating, the influence on the final front velocity should be negligible. Other debris flow models, which do not iteratively adjust viscosity, cannot accurately simulate impacts. Here, our model constitutes a significant improvement, since in the three-dimensional solver we presented, the viscosity bias was reduced by implementing a corrector step: taking the average between the viscosity at the beginning of the time step and the viscosity that corre-

sponds to the velocity field at the end of the time step, the time step is solved again, leading to a better calculation of the velocity. This step can be repeated, according to user specifications, to correct the viscosity several times. Although this procedure increases numerical calculation time, it clearly reduces the time-step dependency of the simulation. Some dependency on the time step is still present when modeling the collapse of material columns, but the origin of this problem is different because it occurs also for Newtonian fluids.

3.2 Effect of grid resolution on rheology

Since the shear rate influences both viscosity models, a strong influence of grid resolution on viscosity results, because the shear rate is averaged over the cell size. For flows over rough topography this may be less critical, but for laboratory flume experiments with thin shear bands the results may depend on grid resolution. When simulating laboratory flume experiments where debris-flow material accelerated in a relatively narrow and short channel (Scheidl et al., 2013), a cell height of 1.5 mm, which is of the order of the laboratory rheometer gap, was still not fine enough to reach the limit of grid sensitivity. The free model parameter τ_{00} influences the shear-rate-dependent term of the visco-plastic rheology model and can be used to adjust the simulation to the grid resolution. As long as the gravel phase and grid resolution do not change, it should be possible to model different water and clay contents based on one calibration test. However, as the composition changes, both τ_y and τ_{00} must change commensurately, since a change in yield stress affects the shear rate. Our procedure for adjusting to different mixtures based on one calibrated test is to perform one iteration step for the yield stress of the new mixture; by calculating τ_y based on the original τ_{00} value from the calibration test but with the new material composition, an updated yield stress of the new mixture is determined. Raising or lowering τ_{00} by the same ratio as the change from the original yield stress of the calibration test to the updated yield stress generates the final τ_y as it is applied to the simulation of the new mixture.

The viscosity of the granular phase is averaged over the cell faces to avoid discontinuous viscosity jumps between cells, which may cause instability due to the sensitivity of incompressible solvers to pressure-dependent viscosity. However, thin cells that allow a precise

calculation of the shear gradient lead to a preferred direction of the smoothing of the granular phase's viscosity which may introduce physically unrealistic behavior. Cell length (in the flow direction), cell width and cell height should at least be of the same order. Especially when front fingering is of interest, a grid resolution test should be carried out, ensuring that front instability is not caused by a large aspect ratio of the cell dimensions.

4 Discussion

Because the purpose of this paper is to illustrate the solver structure and model basis, we defer a detailed discussion of model performance to the accompanying paper, in which the model is validated against laboratory tests, large scale experiments and natural hillslope debris flow events. Here, we discuss only the efficiency of the solver itself, together with a general test about the model accuracy in a gravity-driven open channel flow. The lack of standard benchmark test cases for debris-flow solvers was the motivation to select a numerical test case to compare model speedup between our approach and a closely related drag-force-based Eulerian multiphase model, and to select a well-defined gravity-driven turbulent open channel flow experiment with clear water to inspect the solver validity.

In comparison to drag-force-based Eulerian multiphase models, the Volume of Fluid approach applied here provides significant reduction in calculation time. For an estimate we compared our model with the OpenFOAM standard solver multiphaseEulerFoam. We selected the official tutorial case damBreak4phaseFine, but turned the water phase into mercury to gain a three-phase test case, and applied the standard solver settings from the case to our model. On a CentOS 6.3 Linux machine with 31 GiB memory and sixteen Intel Xeon CPU E5-2665 @ 2.40 GHz processors, our model resulted in a 5.5 times faster calculation with a comparable collapse of the modeled mercury and oil columns (Fig. 5). For the sake of completeness our calculation included one iterative viscosity correction step, thus the model efficiency can be estimated to be about ten times higher than a drag-force-based phase coupling approach.

The model was also applied to an open clear water channel experiment with about 50.6 l/s discharge in a 40 m long and 1.1 m wide rectangular smooth channel with 0.026% inclination (Fischer, 1966). The slurry phase was initialized as water together with a zero gravel phase concentration. A Hybrid URANS-LES model was applied to account for the turbulent flow. Instead of an inlet discharge the model applied periodic inlet and outlet boundary conditions and the flow was driven by gravity. The debrisInterMixingFoam solver predicted the discharge of the turbulent channel flow with an underestimation of 15% and underestimated the corresponding surface elevation by 2.5%. However, the deviations in predicted and measured average flow velocities are probably related to shortcomings of the URANS turbulence model at the bottom boundary, as a comparison between a measured and simulated vertical velocity profile suggests (Fig. 6). Due to the lack of a clearly defined benchmark test case for debris flow models, we have chosen this setup as a well-defined larger-scale laboratory test case where the solver faces varying modeled fluid viscosity due to turbulence.

5 Conclusions

The new debris-flow solver has two main strengths. First, it can model three-dimensional flows and their impact against complexly shaped objects, representing the processes at a high level of detail. Second, its design allows simulating different debris flow material compositions without recalibrating the one free parameter, as long as the simulation grid does not change. Due to the solver's pressure- and shear-dependent rheology, realistic deposit geometries and release dynamics can be achieved, as presented and discussed on the basis of test cases in the accompanying paper. By systematically excluding unknown parameters from the model architecture and by accounting for known flow phenomena in a simplified way, we have developed a debris flow model whose parameters can be roughly estimated based on material composition, leaving only a single calibration parameter. The concept is promising, however important parts of phase interactions are neglected in favor of lower numerical costs and shorter calculation times. The model is still limited to small

simulations of several hundred square meters in surface area unless a powerful computer cluster can be used.

Appendix A: A

The following section describes the detailed implemetation of the PISO iteration procedure as described in Deshpande et al. (2012). By applying the continuum surface force model of Brackbill et al. (1992), the volume integral of eq. 14 is given as

$$\int_{\Omega_i} \frac{\partial \rho \boldsymbol{U}}{\partial t} dV + \int_{\partial\Omega_i} (\rho \boldsymbol{U}\boldsymbol{U}) \cdot \boldsymbol{n} dS = \\ - \int_{\Omega_i} \nabla p_d dV - \int_{\Omega_i} \boldsymbol{g} \cdot \boldsymbol{x} \nabla \rho dV + \int_{\Omega_i} \sigma\kappa\nabla\alpha_1 dV + \int_{\partial\Omega_i} (\mu\nabla\boldsymbol{U}) \cdot \boldsymbol{n} dS + \int_{\Omega_i} \nabla\boldsymbol{U} \cdot \nabla\mu dV. \quad \text{(A1)}$$

The computational domain is discretized into finite-volume cells. Each cell is considered as the owner of exactly one face that it shares with an adjacent neighbor cell, thus each face has a defined owner cell. A surface normal vector S_f with magnitude equal to the surface area of the face is defined on the face pointing outward from the owner cell (Fig. 7). The value at face f of any variable χ calculated in the cell centers as χ_P and χ_N (Fig. 7) can be derived by interpolation using a mixture of central and upwind schemes:

$$\chi_{\mathbf{f}} = \gamma(\chi_P - \chi_N) + \chi_N, \quad \text{(A2)}$$

with a weighting factor γ that can account for the flow direction based on the chosen interpolation scheme and flux limiter. In case of a linear interpolation scheme and a flux limiter ψ, γ can be defined as

$$\gamma = \psi \frac{fN}{d} + (1 - \psi) \frac{\phi_f}{|\phi_f|}, \tag{A3}$$

where d is the distance between the cell centers P and N and fN is the distance from the face center to the cell center N. The face flux denoted as ϕ_f serves as a switch to account for the flow direction since it turns negative when the flow is from N to P (Berberović et al., 2009). Several limiters are implemented (OpenFOAM-Foundation, 2016b); we chose the vanLeer scheme and assumed uniform grid spacing to simplify the following explanations with $fN/d = 0.5$.

Variables that are evaluated at the cell faces are subscripted by f. Due to stability problems that arise from the pressure-velocity coupling in collocated meshes (Ferziger and Peric, 2002), the pressure is solved for the cell centers whereas the velocity is interpolated to the cell faces within the PISO loop.

With the switch function

$$\zeta(\phi_f) = \frac{\phi_f}{|\phi_f|} \tag{4}$$

the velocity $\boldsymbol{U}_f$ at face f can be written based on eq. A2 and A3 as

$$\boldsymbol{U}_f = \frac{\boldsymbol{U}_P}{2}(1 + \zeta(\phi_f)(1 - \psi)) + \frac{\boldsymbol{U}_N}{2}(1 - \zeta(\phi_f)(1 - \psi)), \tag{5}$$

and the corresponding face-perpendicular velocity gradient is given by Deshpande et al. (2012) as

$$\nabla^{\perp}{}_{f}\boldsymbol{U} = \frac{\boldsymbol{U_N} - \boldsymbol{U_P}}{|d|}. \tag{6}$$

At the present time step t^n the phase averaged density of the next time step ρ^{n+1} is known from solving the transport equations. In a first approximation, the corresponding viscosity field μ^{n+1} can be derived accordingly. A simplified formulation of the momentum equation A1 without pressure, surface tension and gravity terms discretized for cell P could then be formulated as

$$\frac{(\rho^{n+1}\tilde{\boldsymbol{U}}) - (\rho^{n}\boldsymbol{U^n})}{\Delta t}|\Omega_P| + \sum_{f\in\partial\Omega_i} \rho^{n}{}_{f}\phi^{n}{}_{f}\tilde{\boldsymbol{U}}_f = \sum_{f\in\partial\Omega_i} \mu^{n+1}{}_{f}\nabla^{\perp}{}_{f}\tilde{\boldsymbol{U}}|\boldsymbol{S}_f| + \nabla\boldsymbol{U}^n\cdot\nabla\mu^{n+1}|\Omega_P|. \tag{7}$$

The tilde stands for the velocity at cell P predicted in the current iterative step, for which eq. 7 yields an explicit expression. For that purpose, eq. 5 and 6 are inserted into eq. 7 using the velocity of the prior iteration step, $\boldsymbol{U^m}$, in all neighbor cells (Deshpande et al., 2012). The explicit expression for the estimated velocity is

$$A_P\tilde{\boldsymbol{U}} = H(\boldsymbol{U^m}), \tag{8}$$

and by including surface tension and gravity this leads to

$$\tilde{\boldsymbol{U}} = \frac{H(\boldsymbol{U^m})}{A_P} + \frac{\sigma\kappa\nabla\alpha_1^{n+1}}{A_P} - \frac{\boldsymbol{g}\cdot\boldsymbol{x}\nabla\rho}{A_P}. \tag{9}$$

The detailed composition of $H(\boldsymbol{U^m})$ and A_P formulated with respect to the splitting between neighbor and owner cells can be found in Deshpande et al. (2012); here it is sufficient to keep in mind that $H(\boldsymbol{U^m})$ contains all off-diagonal contributions of the linear system.

The next step is to assemble the approximated face flux

$$\tilde{\phi_f} = \Big(\frac{H(\boldsymbol{U^m})}{A_P}\Big)_f \cdot \boldsymbol{S}_f + \Big(\frac{(\sigma\kappa)^{n+1}(\nabla^\perp{}_f\alpha_1)^{n+1}}{A_P}\Big)_f |\boldsymbol{S}_f| - \Big(\frac{(\boldsymbol{g}\cdot\boldsymbol{x})^{n+1}(\nabla^\perp{}_f\rho)^{n+1}}{A_P}\Big)_f |\boldsymbol{S}_f| \tag{10}$$

where the subscript f indicates that the variable values at the faces are used. The final flux is found by adding the pressure contribution

$${\phi^{m+1}}_f = \tilde{\phi_f} - \Big(\frac{\nabla^\perp{}_f p_d^{m+1}}{A_P}\Big)_f |\boldsymbol{S}_f|. \tag{11}$$

The sum of the flux over the cell faces needs to be zero due to mass conservation for the incompressible flow

$$\sum_{f\in\partial\Omega_i} {\phi^{m+1}}_f = 0, \tag{12}$$

Thus the pressure is defined by the linear equation system for the updated pressure ${p_d}^{m+1}$

$$\sum_{f\in\partial\Omega_i} \Big(\frac{\nabla^\perp{}_f p_d^{m+1}}{A_P}\Big)_f |\boldsymbol{S}_f| = \sum_{f\in\partial\Omega_i} \tilde{\phi_f}, \tag{13}$$

and can be solved with the preconditioned conjugate gradient (PCG) algorithm, to mention one of several options implemented in OpenFOAM. With the updated pressure ${p_d}^{m+1}$,

the face fluxes ${\phi^{m+1}}_f$ are derived from eq. 11 and the updated velocity filed $\boldsymbol{U}^{m+1}$ is obtained from the explicit velocity correction

$$\boldsymbol{U}^{m+1} = \tilde{\boldsymbol{U}} + \left(\frac{1}{A_P}\right)\left(\sum_{f\in\partial\Omega_i}\frac{(\boldsymbol{S}_f \otimes \boldsymbol{S}_f)}{|\boldsymbol{S}_f|}\right)^{-1} \bullet \left(\sum_{f\in\partial\Omega_i}\left(\frac{{\phi^{m+1}}_f - \tilde{\boldsymbol{U}}_f \cdot \boldsymbol{S}_f}{(\frac{1}{A_P})_f}\right)\frac{\boldsymbol{S}_f}{|\boldsymbol{S}_f|}\right) \tag{14}$$

which is the end of the PISO loop. After updating the index m to $m+1$, the iteration restarts with recalculating H with the updated velocity from equation 8, repeating the loop until a divergence-free velocity field is found.

Code availability

The source-code can be downloaded from the supplement application.zip. Please follow the instructions given in the README.pdf file for installation.

The Supplement related to this article is available online at doi:10.5194/gmdd-0-1-2016-supplement.

Acknowledgements. We thank Shiva Pudasaini, Johannes Hübl and Eugenio Oñate for thoughtful critiques and suggestions.

References

Ancey, C.: Plasticity and geophysical flows: a review., J. Non-Newton. Fluid Mech., 142, 4–35, 2007.

Ancey, C. and Jorrot, H.: Yield stress for particle suspensions within a clay dispersion., J. Rheol., 45, 297–319, 2001.

Balmforth, N. and Frigaard, I.: Viscoplastic fluids: from theory to application, J. Non-Newton. Fluid Mech., 142, 1–3, 2007.

Berberović, E., van Hinsberg, N. P., Jakirlić, S., Roisman, I. V., and Tropea, C.: Drop impact onto a liquid layer of finite thickness: Dynamics of the cavity evolution, Phys. Rev. E, 79, 036 306, doi:10.1103/PhysRevE.79.036306, 2009.

Bohorquez, P.: Study and Numerical Simulation of Sediment Transport in Free-Surface Flow, Ph.D. thesis, Universit"at Malaga, Spain, 2008.

Bohorquez, P.: Finite Volume Method of Falling Liquid Films Carrying Monodispersed Spheres in Newtonian Regime, AIChE J, 58, 2601–2616, 2012.

Bouchut, F., Fernandez-Nieto, E. D., Mangeney, A., and Narbona-Reina, G.: A two-phase shallow debris flow model with energy balance, ESAIM-MATHEMATICAL MODELLING AND NUMERICAL ANALYSIS-MODELISATION MATHEMATIQUE ET ANALYSE NUMERIQUE, 49, 101–140, 2015.

Bozhinskiy, A. N. and Nazarov, A. N.: Two-phase model of debris flow, in: 2nd International Conference on Debris-Flow Hazards Mitigation, pp. 16–18, Teipei, Taiwan, 2000.

Brackbill, J. U., Kothe, D. B., and Zemach, C.: A continuum method for modeling surface tension, J. Comput. Phys., 100, 335–354, 1992.

Brodani-Minussi, R. and deFreitas Maciel, G.: Numerical Experimental Comparison of Dam Break Flows with non-Newtonian Fluids, J. of the Braz. Soc. of Mech. Sci. and Eng., 34-2, 167–178, 2012.

Christen, M., Bartelt, P., and Gruber, U.: RAMMS - a Modelling System for Snow Avalanches, Debris Flows and Rockfalls based on IDL, Photogramm. Fernerkund. Geoinf., 4, 289–292, 2007.

Coussot, P., Laigle, D., Aratano, M., Deganuttil, A., and Marchi, L.: Direct determination of rheological characteristics of debris flow, J Hydraul Eng, pp. 865–868, 1998.

Damián, S. M.: An extended mixture model for the simultaneous treatment of schort and long scale interfaces, Ph.D. thesis, Universidad Nacional de Litoral, Argentina, 2013.

Deganutti, A., Tecca, P., and Genevois, R.: Characterization of friction angles for stability and deposition of granular material, in: Italian Journal of Engineering and Environment: 5th International Conference on Debris-Flow Hazards: Mitigation, Mechanics, Prediction and Assessment, pp. 313–318, Padua, Italy, 2011.

Deshpande, S. S., Anumolu, L., and Trujillo, M. F.: Evaluating the perfomance of the two-phase flow solver interFoam, Computational Science and Discovery, 5, 1–33, 2012.

Domnik, B. and Pudasaini, S.: Full two-dimensional rapid chute flows of simple viscoplastic granular materials with a pressure-dependent dynamic slip-velocity and their numerical simulations, J. Non-Newton. Fluid Mech, 173–174, 72–86, 2012.

Domnik, B., Pudasaini, S., Katzenbach, R., and Miller, S.: Coupling of full two-dimensional and depth-averaged models for granular flows, J. Non-Newton. Fluid Mech, 201, 56–68, 2013.
Ferziger, J. H. and Peric, M.: Computational Methods for Fluid Dynamics, Springer 3rd ed., Berlin, 2002.
Fischer, H. B.: Longitudinal Dispersion in Laboratory and Natural Streams, Ph.D. thesis, California Institute of Technology, 1966.
Forterre, Y. and Pouliquen, O.: Flows of dense granular media, Annu. Rev. Fluid Mech., 40, 1–24, 2008.
Gao, Y. and Li, K.: New models for calculating the viscosity of mixed oil, Fuel, 95, 431–437, 2012.
Guthrie, R., Mitchell, J., Lanquaye-Opoku, N., and Evans, S.: Extreme weather and landslide initiation in coastal British Columbia, Journal of engineering geology and hydrogeology, 43, 417–428, 2010.
Hänsch, S., Lucas, D., Höhne, T., Krepper, E., and Montoya, G.: Comparative simulations of free surface flows using VOF-methods and a new approach for multi-scale interfacial structures, in: Proceedings of the ASME 2013 Fluids Engineering Summer Meeting, Incline Village, Nevada, USA, 2013.
Hilker, N., Badoux, A., and Hegg, C.: The Swiss flood and landslide damage database 1972-2007, Nat. Hazards Earth Syst. Sci., 9, 913–925, 2009.
Hill, D.: The Computer Simulation of Dispersed Two-Phase Flows, Ph.D. thesis, Imperial College, University of London, 1998.
Hirt, B. and Nichols, B.: Volume of Fluid (VOF) Method for the Dynamics of Free Boundaries, Journal of Computational Physics, 39, 201–225, 1981.
Hoang, D., van Steijn, V., Kreutzer, M., and Kleijn, C.: Modeling of Low-Capillary Number Segmented Flows in Microchannels Using OpenFOAM, in: Numerical Analysis and Applied Mathematics ICNAAM 2012, AIP Conf. Proc., vol. 1479, pp. 86–89, Kos Island, Greece, 2012.
Hürlimann, M., McArdell, W., and Rickli, C.: Field and laboratory analysis of the runout characteristics of hillslope debris flows in Switzerland, Geomorphology, 232, 20–32, doi:10.1016/j.geomorph.2014.11.030, 2015.
Imran, J., Parker, G., Locat, J., and Lee, H.: 1D numerical model of muddy subaqueous and subaerial debris flows, J Hydraul. Eng., pp. 959–968, 2001.
Ishii, M.: Thermo-Fluid Dynamic Theory of Two-Phase Flow, Eyrolles, Paris, 1975.
Issa, R.: Solution of the implicitly discretized fluid-flow equations by operator-splitting, J Comp. Phys., 62, 40–65, 1986.

Iverson, R. and Denlinger, P.: Flow of variably fluidized granular masses across three-dimensional terrain: 1. Coulomb mixture theory, J. Geophys. Res., 106, 537–552, 2001.
Jop, P., Forterre, Y., and Pouliquen, O.: A constitutive law for dense granular flows, Nature, 441, 727–730, 2006.
OpenFOAM-Foundation: OpenFOAM Standard Solvers, Website User Guide of OpenFOAM, http://www.openfoam.org/docs/user/standard-solvers.php, visited 12.01.2016., 2016a.
OpenFOAM-Foundation: OpenFOAM Standard Schemes, Website User Guide of OpenFOAM, http://cfd.direct/openfoam/user-guide/fvSchemes/, visited 12.01.2016., 2016b.
Petley, D. N., Hearn, G. J., Hart, A., Rosser, N. J., Dunning, S. A., Oven, K., and Mitchell, W. A.: Trends in landslide occurence in Nepal, Nat Hazards, 43, 23–44, 2007.
Pitman, E. and Le, L.: A two-fluid model for avalanche and debris flows, Philos. Trans. R. Soc. A, 363, 1573–1602, 2005.
Pudasaini, S.: A general two-phase debris flow model, J. Geophys. Res., 117, F03 010, 2012.
Remaitre, A., Malet, J., Maquaire, O., Ancey, C., and Locat, J.: Flow behaviour and runout modelling of a complex derbis flow in a clay-shale basin, Earth Surf Proc Landforms, 30, 479–488, 2005.
Renardy, M.: Some remarks on the Navier-Stokes Equations with a pressure-dependent viscosity, Comm. in Partial Differential Equations, 11, 779–793, 1986.
Schatzmann, M., Fischer, P., and Bezzola, G. R.: Rheological Behavior of Fine and Large Particle Suspensions, J. Hydraul Eng.-ASCE, 796, 391–430, 803.
Scheidl, C., Chiari, M., Kaitna, R., Müllegger, M., Krawtschuk, A., Zimmermann, T., and Proske, D.: Analysing Debris-Flow Impact Models, Based on a Small Scale Modelling Approach, Surv. Geophys, 34, 121–140, 2013.
v. Boetticher, A., Turowski, J. M., McArdell, W. B., Rickenmann, D., Hürlimann, M., Scheidl, C., and Kirchner, J. W.: (submitted) DebrisInterMixing-2.3: A Finite Volume solver for three dimensional debris flow simulations based on a single calibration parameter. Part two: Model validation, Geoscientific Model Development, 2015.
Yu, B., Ma, Y., and Qi, X.: Experimental Study on the Influence of Clay Minerals on the Yield Stress of Debris Flows, J. Hydraul. Eng., 139, 364–373, 2013.

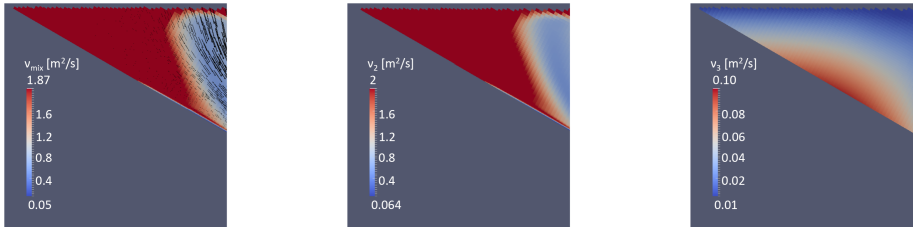

Figure 1. Viscosity distribution (indicated by color scale) along a 28 cm long section through the modeled 0.01 m^3 release block 0.2 s after release, corresponding to the experimental setup of Hürlimann et al. (2015). The starting motion (black velocity arrows) with corresponding viscosity distribution of the mixture (left) is a consequence of blending pure shear-rate dependent slurry-phase rheology (center) with the pressure- and shear-rate-dependent gravel phase rheology that accounts for Coulomb friction (right). Because the gravel concentration in this example is low, its effect on the overall viscosity is small.

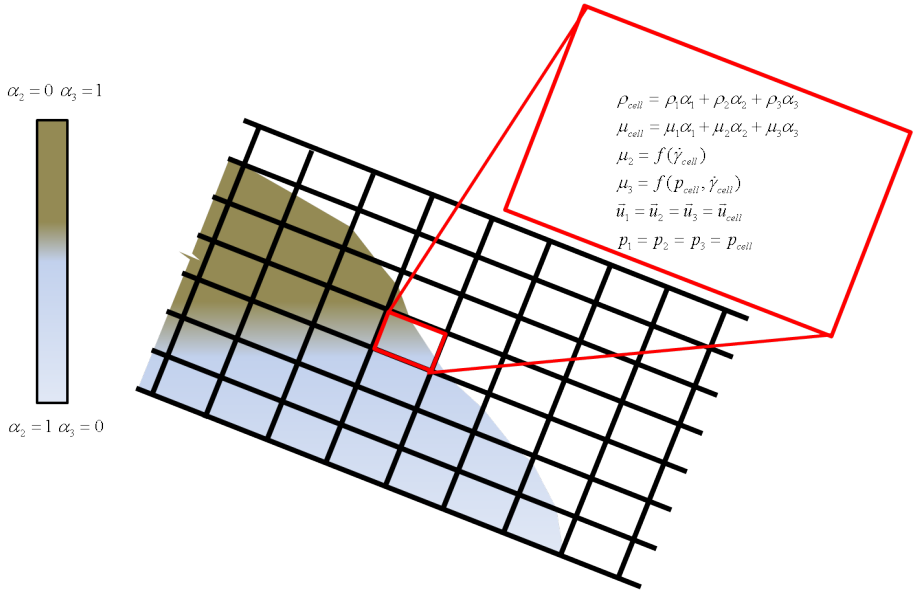

Figure 2. Longitudinal section through a debris flow front discretized with finite volume-cells, showing the constitutive equations for one cell with density ρ and viscosity μ given the densities $\rho_{1..3}$, viscosities $\mu_{1..3}$ and proportions $\alpha_{1..3}$ of phases present. 1 denotes air (white colored cell content), 2 the mud and 3 the gravel phase, respectively.

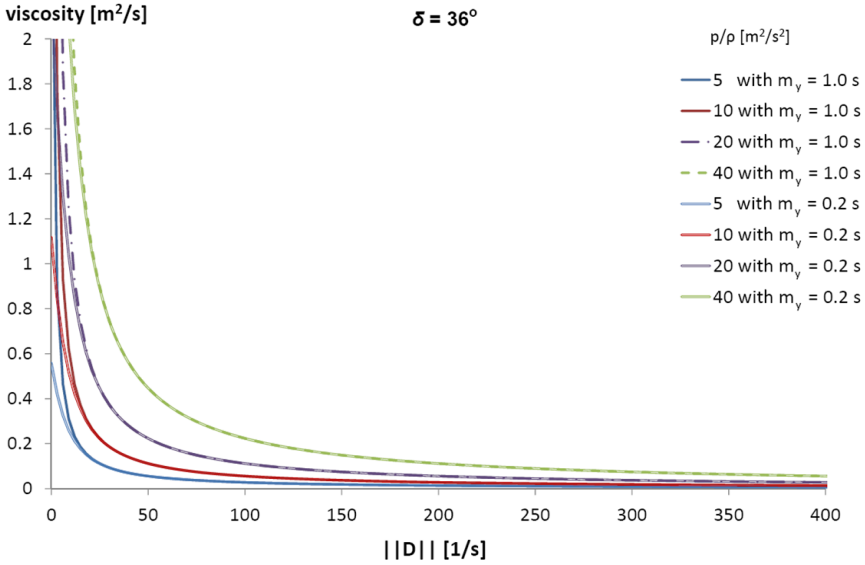

Figure 3. Dependency of the kinematic gravel phase viscosity ν_s (normalized by density) on the norm of the strain rate tensor $||D||$ at different levels of pressure normalized by density, for $m_y = 1$ s and $m_y = 0.2$ s and a friction angle $\delta = 36°$.

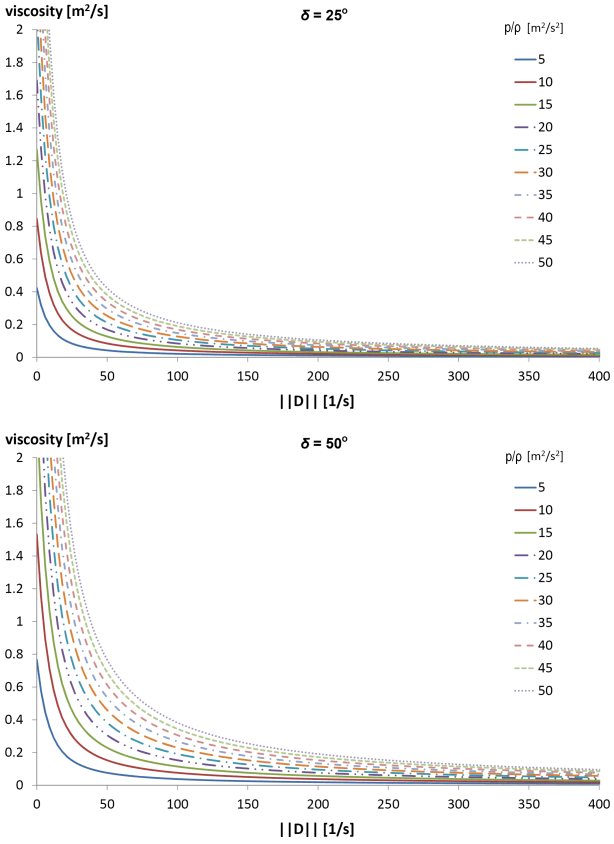

Figure 4. Dependency of the kinematic gravel phase viscosity (for friction angle $\delta = 25^\circ$ and 50°) on the norm of the strain rate tensor $||D||$ at different levels of pressure normalized by density, for $m_y = 0.2$ s.

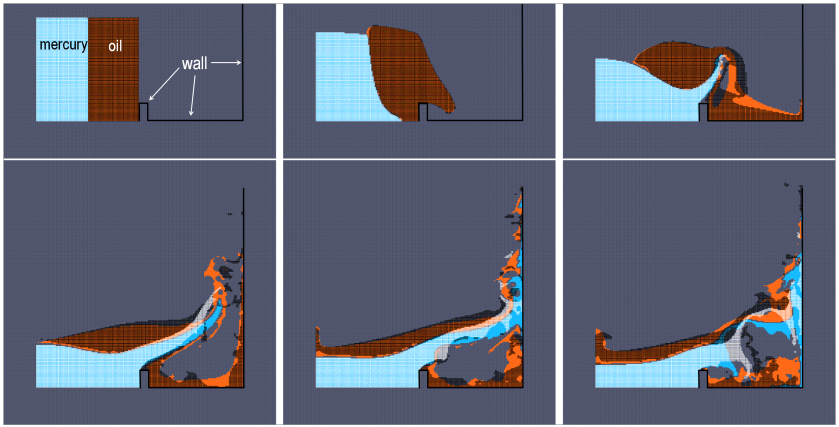

Figure 5. Phase positions in a dam break standard test-case simulation using a drag-based three phase multiphaseEulerFoam simulation (air is transparent, blue indicates mercury and orange represents oil) as background shapes with the corresponding phase positions of our model as wire frame in front (with white mercury as slurry phase and black oil as gravel phase). The visualized time steps correspond to 0, 0.1, 0.2, 0.3, 0.4 and 0.5 seconds.

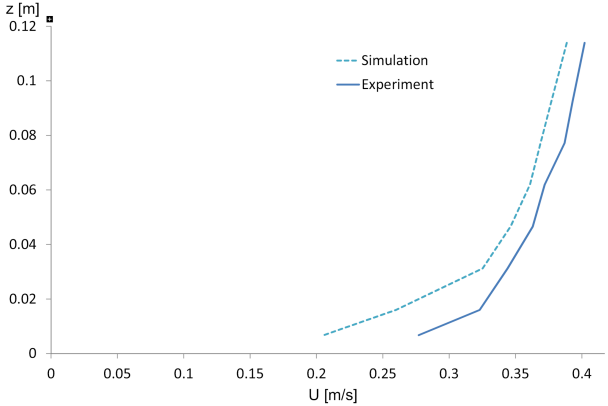

Figure 6. Comparison of simulated and measured average vertical velocity profiles 27 cm away from the channel sidewall of a 1.1 m wide and 40 m long rectangular channel with smooth surface (z is the corresponding height above the bed). In the experiment (Fischer, 1966), a 50.6 l/s inlet discharge was combined with a 0.026% channel inclination resulting in 12.8 cm average flow depth. The simulation applied periodic inlet and outlet boundary conditions and a symmetry plane at the channel center line. Additional calibration of the turbulence model may improve the result.

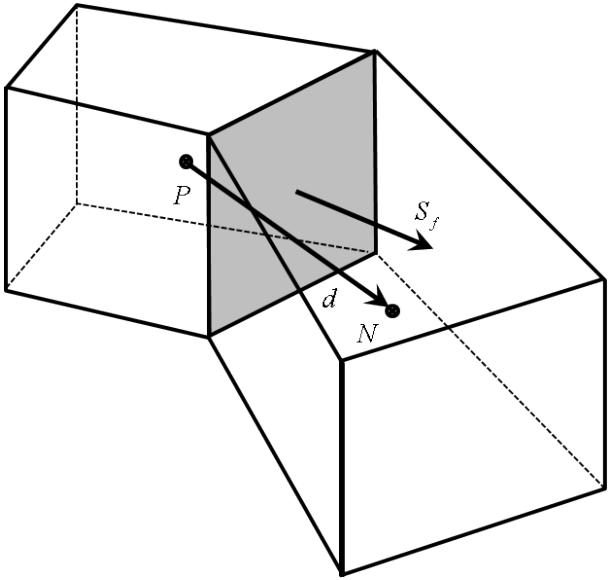

Figure 7. Sketch of two adjacent cells P and N and the shared face f owned by cell P. S_f is the face surface normal vector while d denotes the distance vector from cell center P to cell center N.